Appendix B: Simulation of the Blade Manufacturing Process

This appendix discusses the step-by-step process of the modeling of the CX-100 wind turbine blade for the manufacturing process and the resulting structural behavior of the cured composite system. Section 1 focuses on the forming of the various layers into each mold of the blade and the analysis of the fabric stresses and in-plane waviness of the yarns as they conform to the shape of the mold. Section 2 shows how the simulation can be used to predict the formation of out-of-plane wave defects. The effect of out-of-plane wave defects on the structural stiffness of the blade and on the compressive strength of coupon samples is also studied.

The manufacture of the CX-100 wind turbine blade consists of hand-laying several layers of fabric and balsa core material into the molds, followed by a vacuum pressure to first compact the layers and then infuse each mold with resin. The fully cured LP and HP sides are then bonded with a spar cap to create the full wind turbine blade.

In the finite element model for the manufacture of the blade, the hand layup of fabric layers is simulated by using a rigid core (punch) to press the fabric into the fixed, rigid mold (Figure B-1). The punch is allowed to move only in the vertical direction. Additionally, rigid binders which can translate vertically, provide in-plane tension in the fabric to prevent folding and sliding of the fabric layers as they are pressed into the mold by the punch. This forming simulation is done using the explicit formulation in Abaqus which was chosen for computing time efficiency, relatively robust contact algorithms and the option to account for the mechanical behavior of the fabrics via user-defined material models. To save computation time, layers are pressed into each mold in groups. After

initially being pressed into the mold using the rigid punch, additional pressures are subsequently applied to press the layers tightly into each mold.

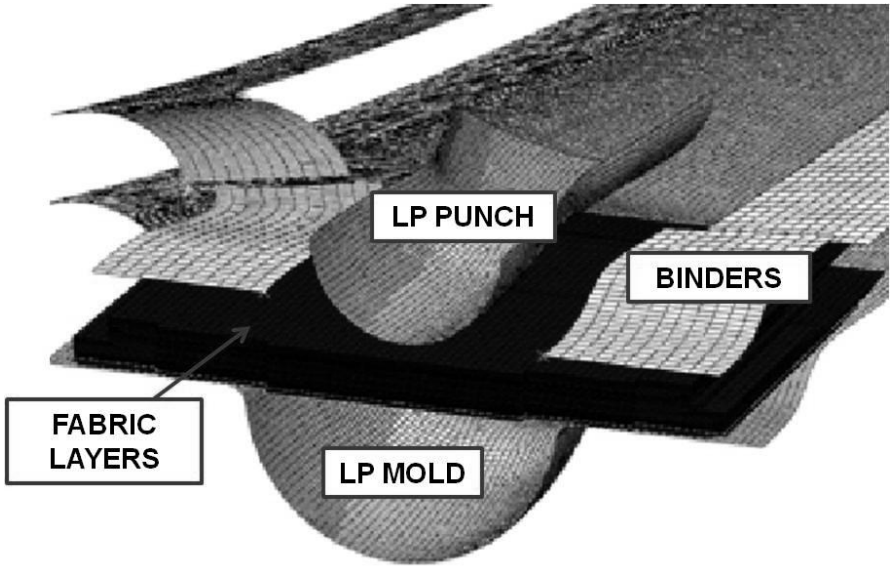

Figure B-1. Punch pressing fabric layers into the LP mold. Binders are used to provide in-plane tension in the fabric

After all of the layers of fabric have been pressed into the molds, the compaction of the fabric layers is simulated by applying a pressure equivalent to atmospheric pressure directly onto the surface of the top layers. It is during this stage in the manufacturing process that fabric layers may bunch together to form out-of-plane wave defects that eventually compromise the performance and reliability of wind turbine blades [1]. Because the formation of wave defects most likely occurs during the hand layup and vacuum compaction stages of the manufacturing process, the resin infusion process is not simulated in this research. Instead, it is assumed that once the layers of fabric have been placed in the molds, the resin is evenly distributed across each mold with a fiber volume fraction of 55%, which is typical for the CX-100 blades manufactured using the SCRIMP® process [1]. After the LP and HP molds are

individually modeled, they are bonded together with tie constraints, resulting in the full CX-100 blade model.

1 FORMING SIMULATIONS

Forming simulations were conducted to explore the deformation of the fabrics, specifically the reorientation of the fabric yarns, and the fabric stresses during the hand layup stage of the manufacturing process. These simulations serve as a design tool to determine the number of layers and fabric orientations for drapability as well as for structural stiffness. The fabric layers of CX-100 blade are currently placed by hand. However, for this research, the fabric layup process was completed using a rigid mold paired with a matched core. The intent of using the matched tools was to simulate the hand layup process to investigate if and where defects could be developed in the blade and to investigate the potential for automating the forming process.

The forming simulations initially consisted of fixed rigid molds for the low-pressure (LP) and high-pressure (HP) sides of the blade and matching rigid cores to press the fabric layers into the molds. Using SolidWorks, the CAD model of the CX-100 blade provided by TPI Composites was divided into two parts to represent the LP and HP molds (Figure B-2).

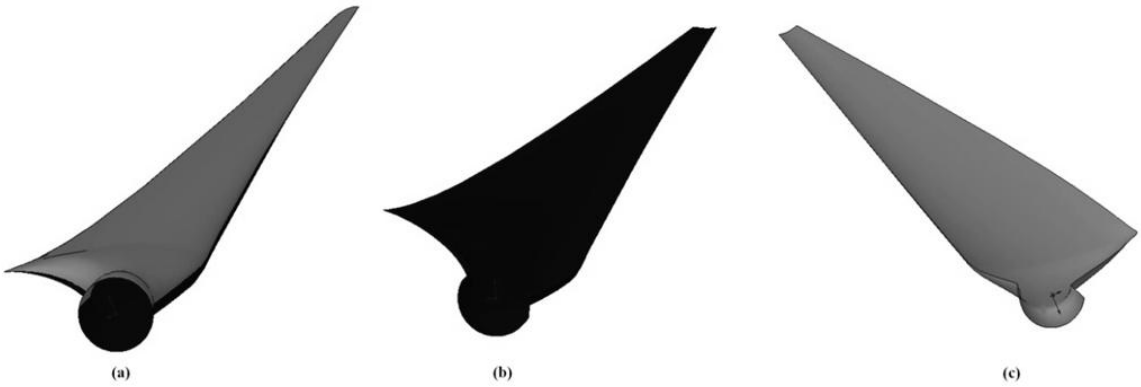

Figure B-2. CAD model of (a) CX-100 blade split into (b) LP mold and (c) HP mold

The rigid mold geometries were scaled down based on the radius of the root sections to create cores that could accommodate the thickness of the layers that would be pressed into each mold (Figure B-3). The molds and cores were meshed with enough resolution of rigid shell elements to maintain smooth curvatures. Figure B-4 shows that without sufficient resolution, the mold surfaces would be jagged and the fabric layers would subsequently conform to those jagged surfaces.

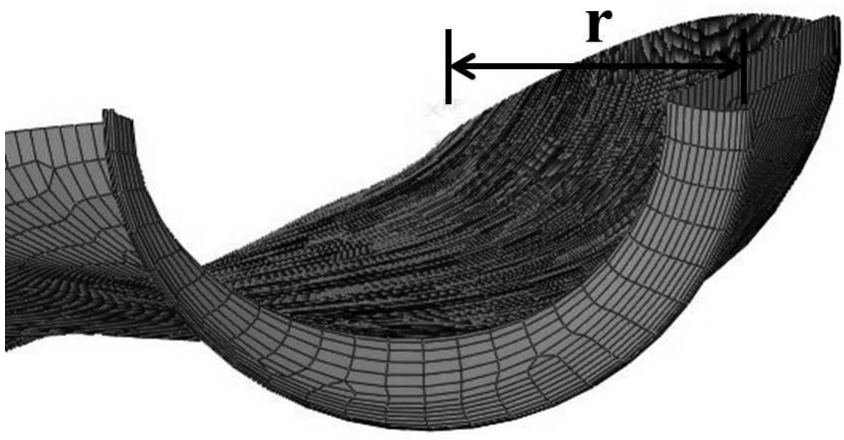

Figure B-3. Scaling of rigid cores for forming simulations

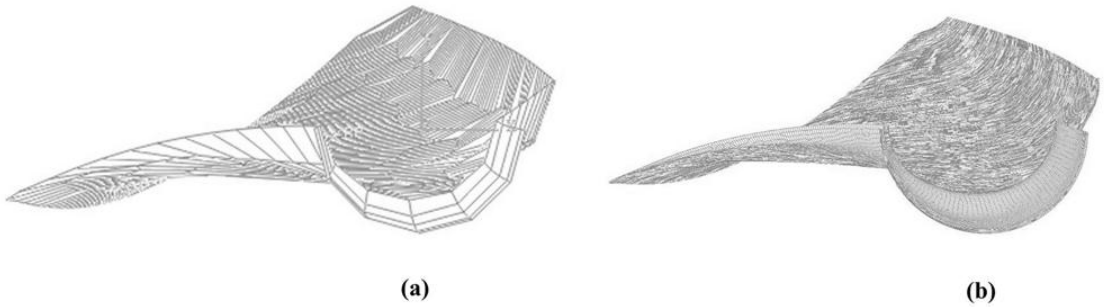

Figure B-4. CX-100 tooling meshed using rigid shell elements with (a) insufficient resolution and (b) sufficient resolution

In the layup of the CX-100 blade, a gelcoat initially covers the entire inner mold surfaces. This gelcoat is then covered by a mat of random chopped fibers, followed by the double-bias fabric, E-BXM 1708. Another double-bias fabric, E-BXM 1208, is then laid into the root section and a portion of the blade skin section, as shown by the shaded region in Figure B-5. For the forming simulation, the deformation of these first four fabric layers was insignificant and defects were not formed in these layers [1]. The thickness of the first four layers was considered in the finite element model by using the built-in Composite Ply feature in Abaqus. The ply-stack plot shown in Figure B-5 shows the thickness and the fiber orientations of each of the first four layers.

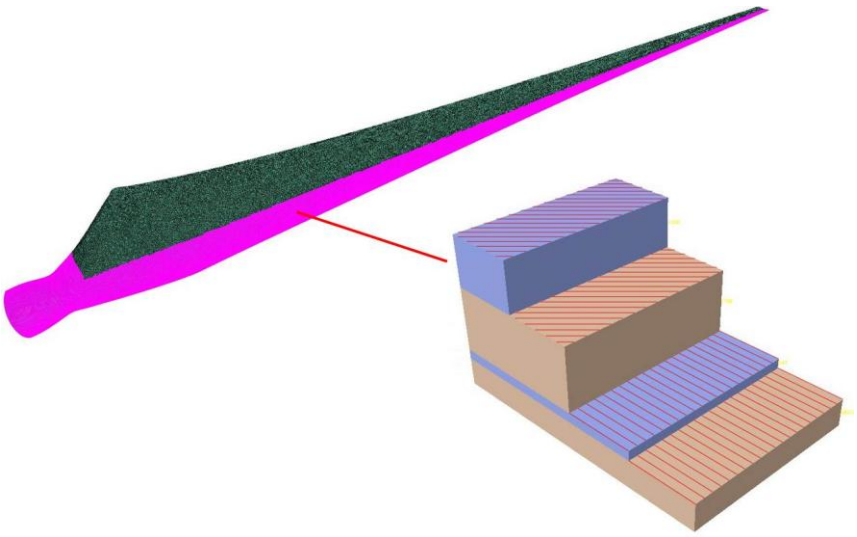

Figure B-5. Ply-stack plot of first four layers including the highlighted region of the E-BXM 1208 fabric layer

With the thickness of the first four layers laid into the mold, the placing of the 46 root layers was simulated next. During the manufacturing process, fabric layers are laid into a mold individually by hand. However, to simulate the placing of layers individually, the core surface would need to be changed each time to account for the changing thickness due to additional plies, i.e. the effective radius of the sections of the core would be reduced with the addition of each ply. Therefore, to save time, all of the fabrics were pressed into the root section of each mold simultaneously, and the core was scaled accordingly one time to account for the thickness of all of the root layers. To prevent folding and sliding of the fabric layers as they were pressed into the mold, flanges were added to the molds with matching rigid binders to provide in-plane tension in the fabric layers. This in-plane tension is analogous to the hand stretching of the fabric layers as they are manually positioned in the mold during the layup process. Because of ply drops in the root section, the effective overall thickness tapers down as viewed from

the root of the blade looking to the tip, and thus the binders were segmented (Figure B-6b) to maintain binder contact along the tapered plane, as shown in Figure B-6a. Otherwise, a continuous binder would provide in-plane tension in the thickest section but would not induce such tension in areas where the thickness had decreased.

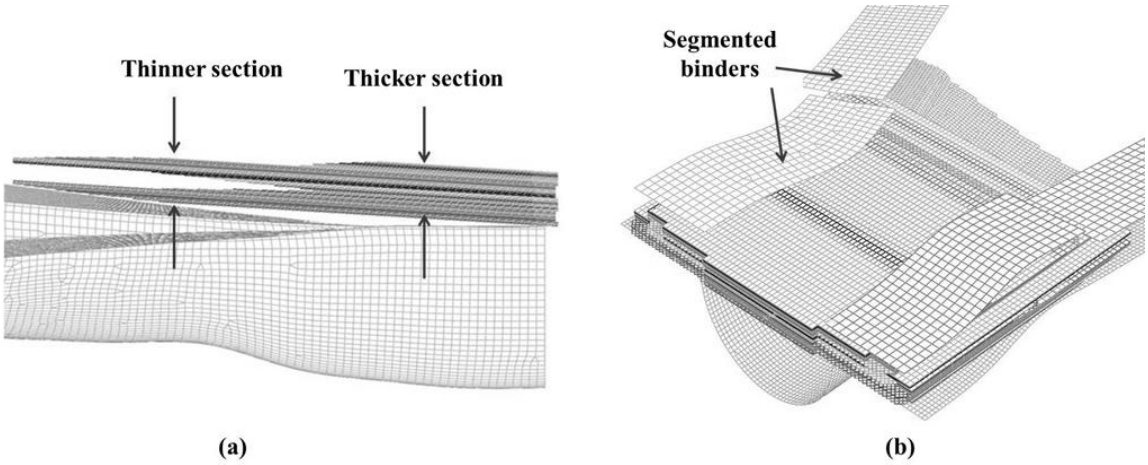

Figure B-6. Forming simulation with (a) varying root-layer sizes requiring (b) segmented binders

In addition to the flanges and binders added to the molds to accommodate the "automated" manufacturing process, the intersection area between (Figure B-7a) the trough of the molds and flanges was rounded (Figure B-7b) to prevent convergence issues that could arise as elements attempted to wrap around what would otherwise have been sharp edges as shown in Figure B-7a. To keep the curvature of the rounded edges smooth, the mesh of the mold in Figure B-7b was also refined.

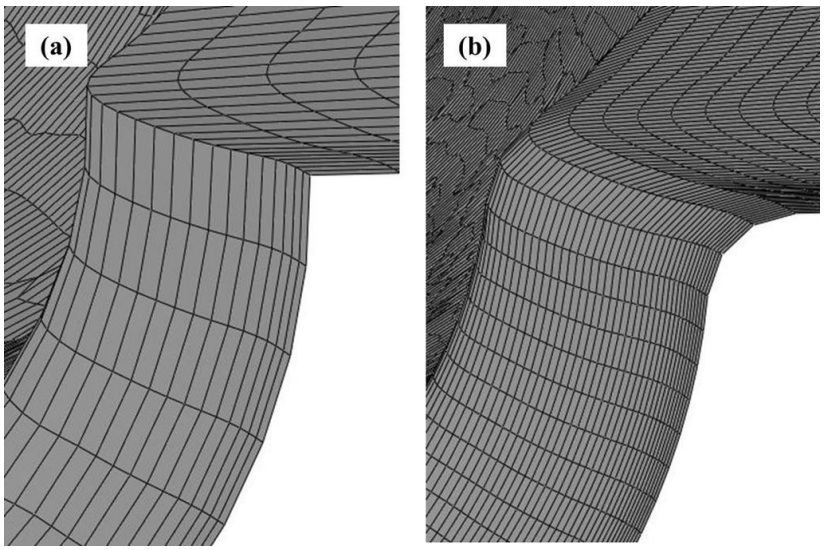

Figure B-7. Flanges added to rigid mold with (a) sharp edges changed to (b) rounded edges to allow fabrics to drape more easily

After the simultaneous forming of the 46 root layers, the molds with the flanges and binders were replaced by the molds without the flanges. Pressures were applied to the surfaces of the root layers preceding the first three spar cap layers to press them tightly into the molds. Once sitting firmly in the mold, the nodes of those root layers were fixed into place, as shown in Figure B-8a, and the first three spar-cap layers were formed using a combination of rigid cores (Figure B-8b) and additional pressure (Figure B-8c). Note that a multi-piece core was used because the thickness at the skin of the blade was much less than that at the root section and a single-piece core would not be able to press the spar-cap layers fully into the mold in the skin section. Pressure could be applied uniformly over the entire spar-cap surface or over different regions such as the root section shown in Figure B-8c, depending on how well the layers were pressed into the mold by the rigid cores.

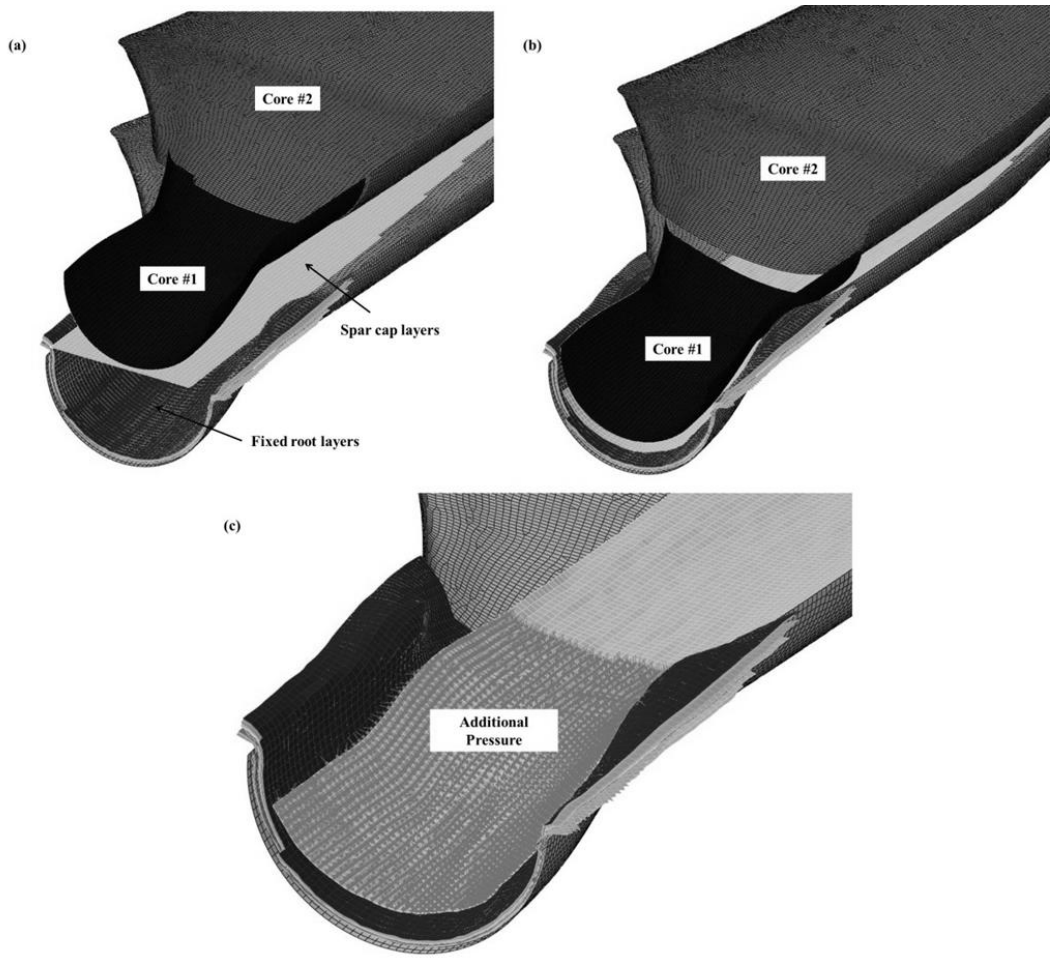

Figure B-8. (a) Forming of spar cap layers using (b) rigid cores and (c) additional pressure

During the forming of the spar-cap layers, the low shear stiffness of the double-bias fabric, E-BX 0900, led to the distortion of some shell elements (Figure B-9a). In such cases, tensile forces were applied to the edges of the fabric in an effort to straighten the elements (Figure B-9b) and then pressures were reapplied to press the fabric down into the mold. This combined step of in-plane tension and downward pressure was analogous to the manipulation of the fabric done by hand by operators on the manufacturing floor and to what would need to be done if the process were to be automated.

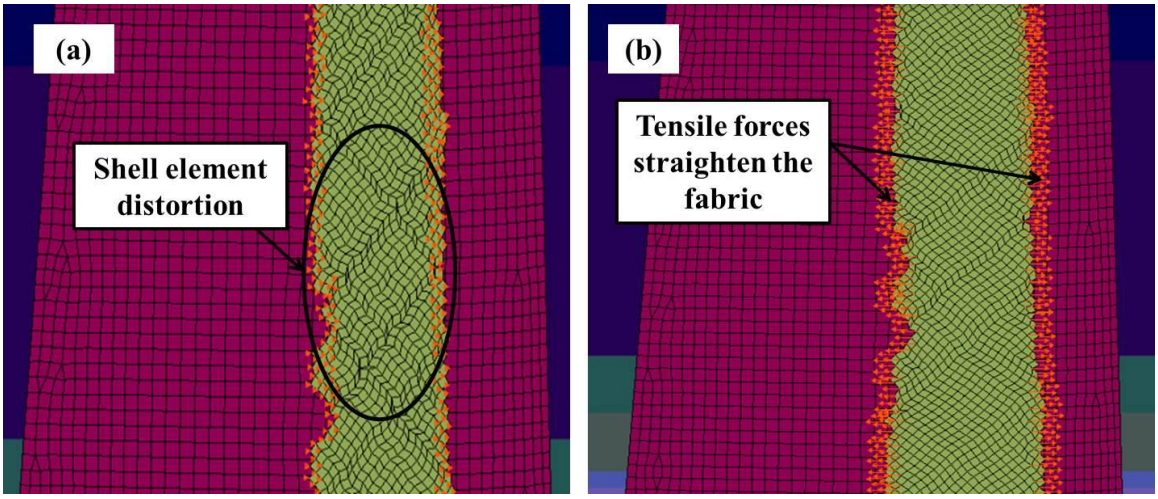

Figure B-9. (a) Forming of a double-bias spar-cap layer leading to element distortion. (b) In-plane tension is applied to straighten the fabric

After the forming of the spar-cap layers was complete, the nodes of the spar-cap layers were also fixed in place and the root layers preceding the next group of spar-cap layers (layers 36-39) were imported into the model. Pressures were applied to those layers to press them tightly into the mold. The nodes of those layers were then fixed into place along with all other previously formed layers, and the next group of spar-cap layers was formed using the same approach presented for the first three spar-cap layers. Likewise, the remaining root layers that were laid up after spar-cap layers 36-39 were tightly pressed into the mold as presented in the case of the other root layers. The resulting LP and HP molds each included the thicknesses of the first four layers, the 46 root layers, and the seven spar-cap layers. All of the excess fabric that was originally clamped at the flanges was cut away such that all of the material sat inside the molds and did not hang over the edges (Figure B-10). The insertion of the shear web and the balsa

core material and the assembly of the LP and HP molds are discussed later in this appendix.

Figure B-10. Formed layers in (a) LP mold and (b) HP mold

During the forming simulations, the fabric stresses of each individual layer were examined to determine if any problematic areas existed as a result of the fiber reorientations and stretching. In particular, in-plane shear angle contours were observed to see if any yarns had trellised beyond the locking angle that might lead to out-of-plane buckling. Also, the tensile forces in the yarns were examined to indicate if any yarns were in danger of breaking. The limits of the shear angle contours were based on the locking angles determined from the fabric-characterization shear-frame tests, and the limits of the tensile force contours were based on the yarn fracture loads. This draping analysis of the LP and HP molds did not indicate excessive shearing of the fabric in any particular areas, nor were any yarns in danger of breaking due to high tensile loads.

Figure B-11a shows the shear angle contours in a biaxial HP root layer with the maximum shear angle set to the locking angle of 36^{o}. For the most part, the yarns remain oriented in their intended directions, as indicated by the blue regions and the annotations.

However, despite little in-plane shearing, the contours still indicate that the shearing is not uniform throughout the part. Structurally, a zone-based or ply-based modeling approach could not account for the nonuniform shearing without the use of knockdown factors or by breaking the zone into many smaller zones, thereby making the defining of the property variations a very tedious task.

Note in Figure B-11b that the yarns of a double-bias fabric also did not shear significantly in the root section. While the double-bias fabrics do not necessarily have a locking angle, as is defined for the biaxial fabrics, the contours in Figure B-11b show that the yarns did not deviate much from their intended ±45^{o} orientations. However, some slight in-plane waviness is observed, as shown in the zoomed-in view of the double-bias fabric in Figure B-12.

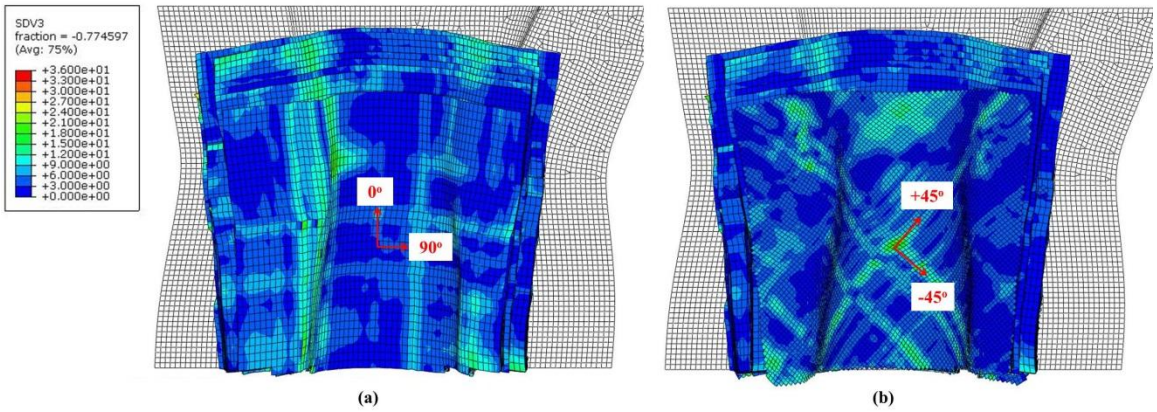

Figure B-11. In-plane shear angle contours in a (a) 0/90 biaxial fabric and (b) +/-45 double-bias fabric

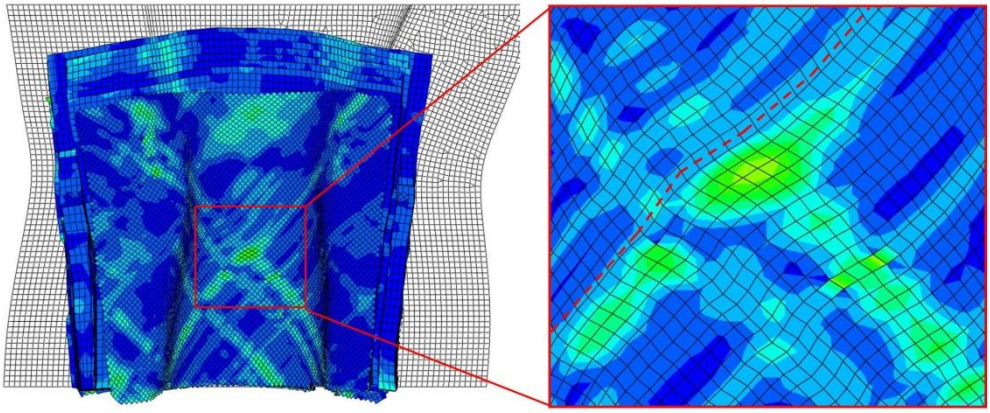

Figure B-12. Zoomed-in view of double-bias fabric showing slight in-plane waviness of yarns

Similarly, typical tensile-load contours from a biaxial root layer (Figure B-13a) and a double-bias root layer (Figure B-13b) indicate that none of the yarns experienced tensile forces beyond their respective fracture loads. The areas annotated in Figure B-13b that show high tensile forces are in the excess fabric flange regions which are later cut from the fabric.

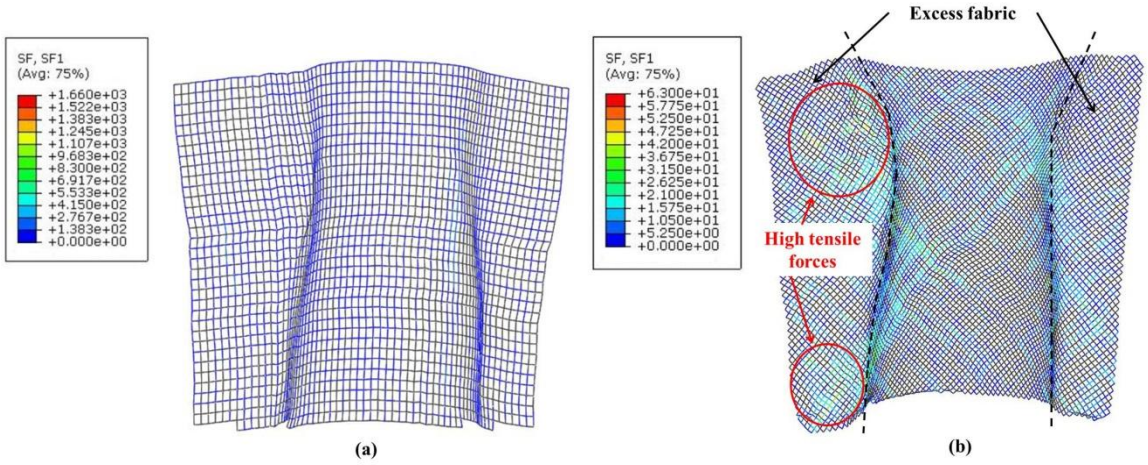

Figure B-13. Yarn tensile force contours in a (a) 0/90 biaxial fabric and (b) +45°/-45° double-bias fabric

Figure B-14 shows the workers cutting away the excess material after the fabric has been placed in the mold. Using the forming simulation methodology of the current research, the initial fabric blank sizes, or flat patterns, can be optimized to reduce the amount of excess fabric that must be cut prior to placement in the mold in either a manual or automated composite manufacturing process.

Flat pattern optimization could help reduce material costs and the time needed to cut away excess material. After first running a forming simulation with an oversized blank, the "ideal" blank geometry can be extracted, as indicated by the path of nodes in Figure B-15a. A second forming simulation, shown in Figure B-15b, is done to validate the "ideal" blank size such that no excess fabric will exist after pressing the layer into the mold.

Figure B-14. Manual cutting of excess fabric during the manufacturing process

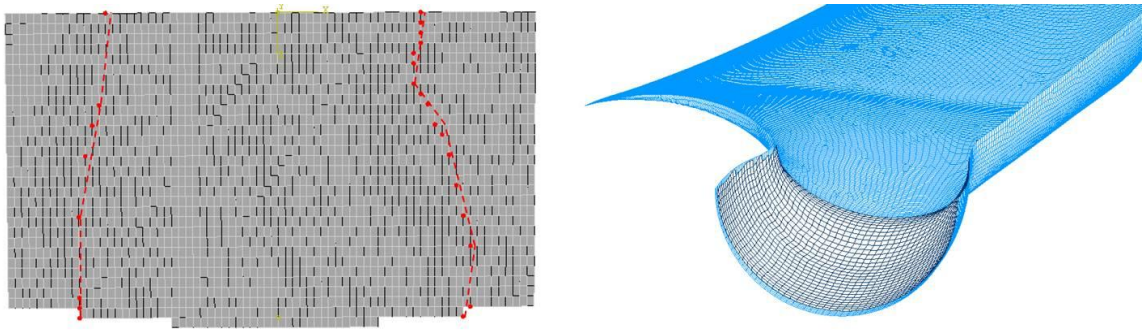

(a) (b)

Figure B-15. Flat pattern with (a) node path from deformed fabric to determine where to cut the fabric for (b) minimal excess material after forming

2. VACUUM COMPACTION AND BLADE ASSEMBLY

After the forming simulations and draping analyses were complete, a pressure equivalent to atmospheric (101 kPa) was applied to the top-fabric surfaces to simulate the compaction of the layers during the manufacturing process via a vacuum bag. It is during this stage that layers of fabric can potentially bunch together to form out-of-plane waves that are later filled with resin to form resin-rich pockets. After simulating the vacuum compaction on the LP and HP halves, the two halves were assembled to create a complete model of the cured-composite CX-100 wind turbine blade, which is ready for use in structural analyses.

2.1 Out-of-plane Wave Defects

Composite wind turbine blade manufacturers have been challenged as to avoid the formation of wave-defects. Manufacturers have expressed the desire for a high-fidelity simulation such as the one proposed in this research that can provide insight into where defects may form and what mechanisms are responsible for their formation. Note,

however, that such defects are not a concern in the CX-100 blade, and therefore the forming simulations presented in this research were not expected to predict wave defects in any particular location [1]. In fact, upon the application of vacuum pressure, the simulation confirmed that there was no out-of-plane deformation in either the LP or HP mold. However, to demonstrate the usefulness of the proposed methodology for predicting wave defects, variations in the bending stiffness and interlaminar friction were made in the spar-cap layers of the LP mold. These simulations focused on the spar cap to coincide with the focus of a separate study in which manufactured wave defects were embedded in the spar cap of an actual CX-100 [2, 3]. The simulations are summarized in Table B-1. Note that $\boldsymbol{EI}$ represents the bending stiffness of the fabric and μ_s, μ_d and β represent the static coefficient of friction, dynamic coefficient of friction, and exponential decay constant, respectively.

Table B-1. Parametric study on wave defect formation in CX-100 spar cap

Simulation No.	EI (N-mm^2)	μ_s	μ_d	β
1	300	0.93	0.57	1.0
2	3	0.93	0.57	1.0
3	300	0.30	0.25	0.7
4	3	0.30	0.25	0.7

Simulations 1 and 2 varied the fabric bending stiffness while maintaining the static and dynamic friction coefficients equal to those measured when using tackifying spray. Simulation 1 used the actual bending stiffness of the carbon NCF (300 N-mm^2) while Simulation 2 used the lowest measured bending stiffness value of 3 N-mm^2 from the fabric characterization. After the application of atmospheric pressure, the spar-cap

layers remained undeformed using these combinations of bending stiffness and friction. The contours in Figure B-16 represent out-of-plane displacement in units of mm. The upper contour limit of displacement (4 mm) was based on the amplitude of typical defects found in wind turbine blades [1]. Note the lack of any significant out-of-plane displacements when using the 4-mm max as a reference.

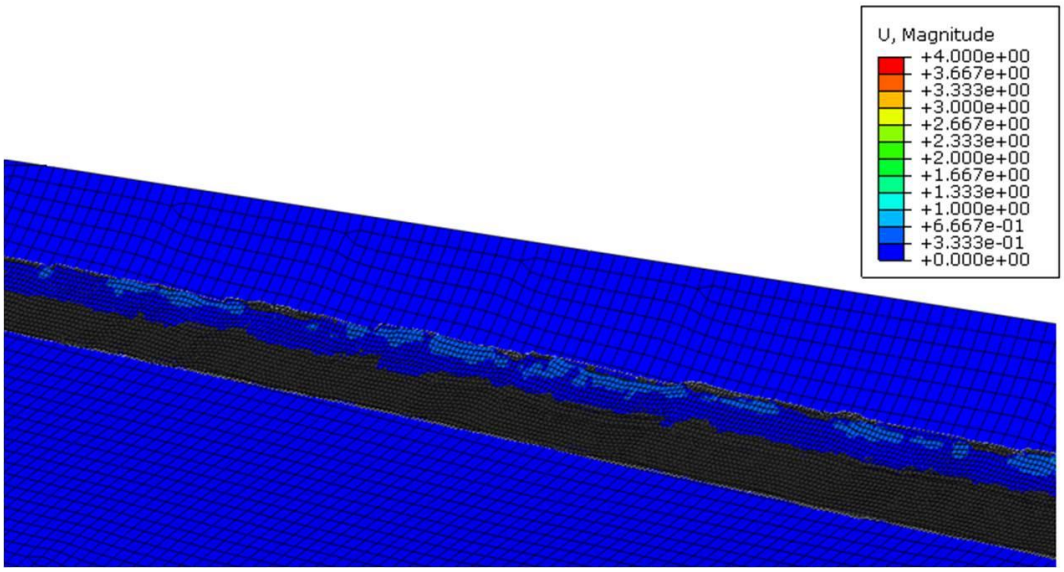

Figure B-16. CX-100 spar cap without out-of-plane deformation (Simulation #1)

Simulations 3 and 4 used the same bending stiffness values as were used in the first two simulations but used lower coefficients of friction representing the Coulomb friction measured without the tackifying spray between the carbon and E-Glass spar-cap fabrics. When defining lower friction coefficients with the stiffer fabric in Simulation 3, no out-of-plane deformation was observed, but the combination of low bending stiffness and low friction coefficients in Simulation 4 led to the formation of a wave at the 6.7-m spanwise location. The wave did not propagate across the entire width of the spar cap (Figure 17).

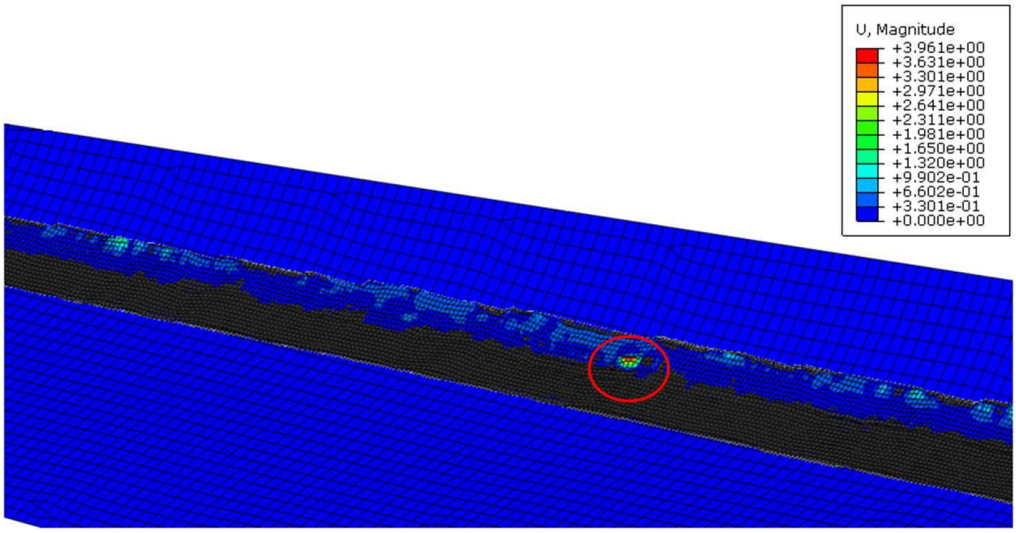

Figure 17. CX-100 spar cap with out-of-plane deformation (Simulation #4)

According to the contour plot in Figure 17, the height of the wave defect was 3.96 mm, which falls within the range of typical defect heights found in wind turbine blades. However, because the mesh density of the fabric layers in the blade model is chosen to allow for reasonable computational times, too coarse a mesh can compromise the resolution and thereby compromise the ability of the model to predict accurately the size, location and severity of a defect. When such a defect is observed using a coarse mesh, then mesh refinement is suggested to improve the resolution of the prediction of the defect formation.

Figure B-18 shows the out-of-plane displacement contours in the spar cap in units of mm. These contours are the result of applying a vacuum pressure using the same parameters as those used in Simulation 4, but with a coarser mesh. Although some out-of-plane deformation is still observed at the 6.7-m location, the contours indicate that the wave height is over two times the height (7.983 mm) cited in Figure 17. Furthermore, out-of-plane deformations that are most likely singularities as a result of poor mesh

resolution are shown in multiple areas along the spar-cap length. Figure B-18 shows the importance of having a sufficient mesh when performing simulations of the manufacturing process.

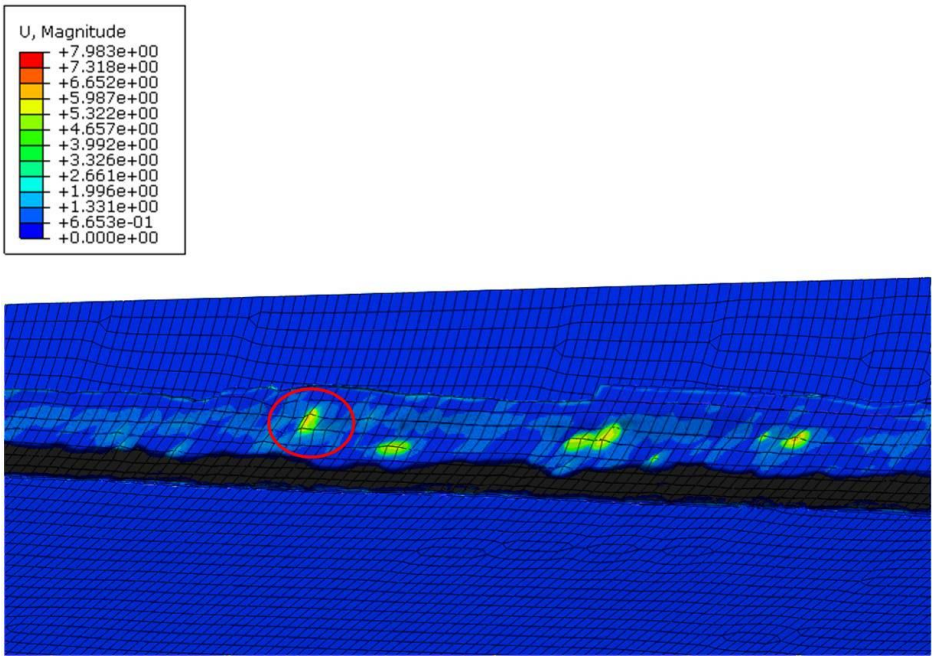

Figure B-18. Coarse spar-cap mesh showing out-of-plane deformation with insufficient mesh refinement

As an example of how the methodology presented in this research could be extended to other blade designs, a hypothetical ply stack-up in the root section of the HP mold was generated such that a large ply drop of 15 mm existed for a total of 27 layers, as shown in Figure B-19. After being formed into the mold using a rigid core and additional pressure, the fabric layers sat tightly in the mold (Figure B-20). Other than at the location of the ply drop, no other out-of-plane waviness was observed in the layers. However, upon application of a vacuum pressure onto the top fabric surface, some of the fabric layers began to buckle out-of-plane toward the back end of the root, as denoted by the circled area in Figure B-21. This type of simulation could assist designers in how to

distribute ply-drops more evenly in the root area, such as in the case of the CX-100, so as to avoid the formation of wave defects.

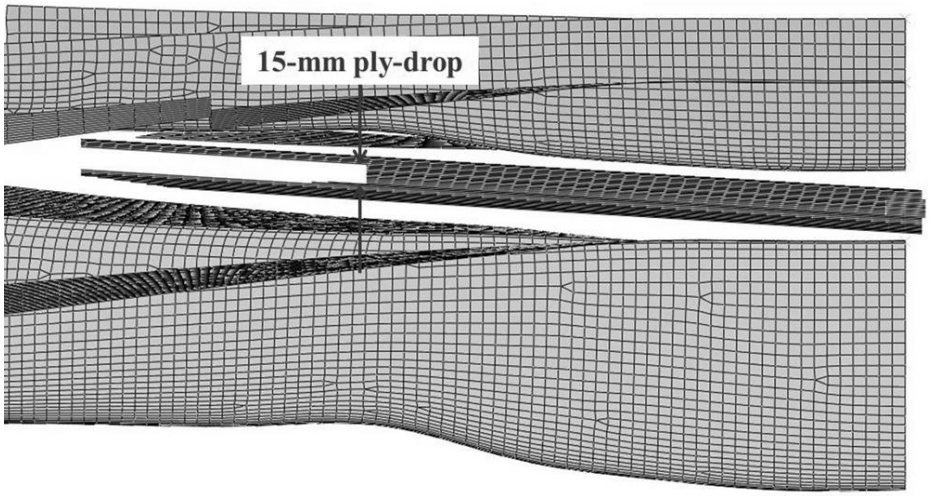

Figure B-19. Hypothetical HP root build-up including a 15-mm ply drop

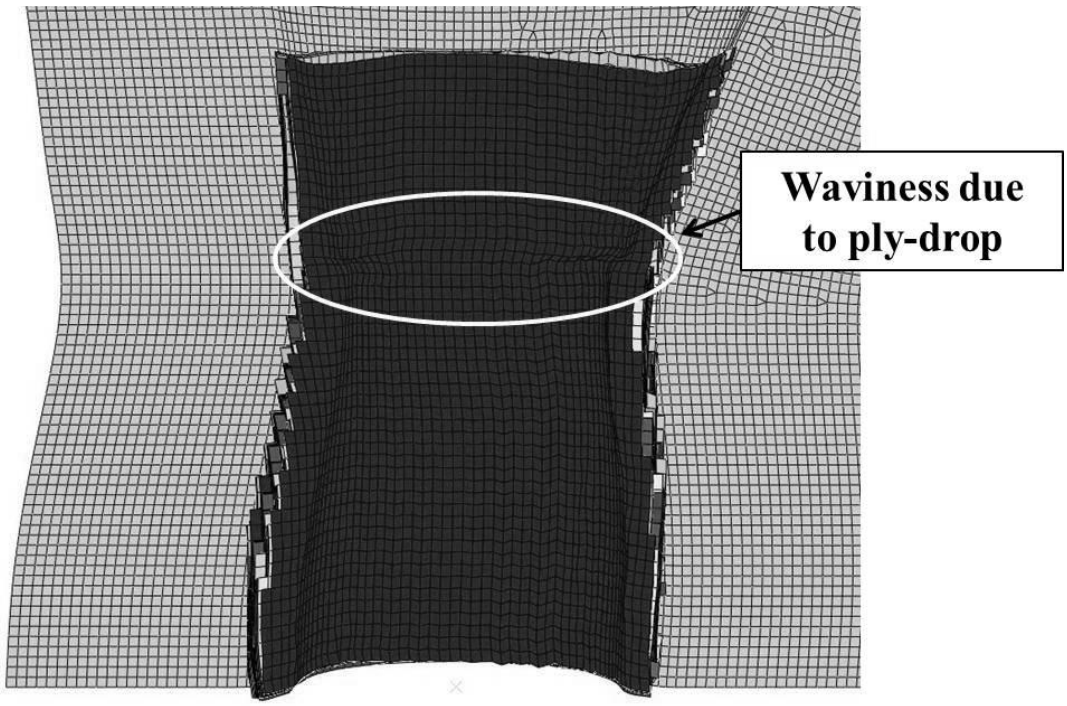

Figure B-20. Wave defect in root section after forming and prior to the application of vacuum pressure

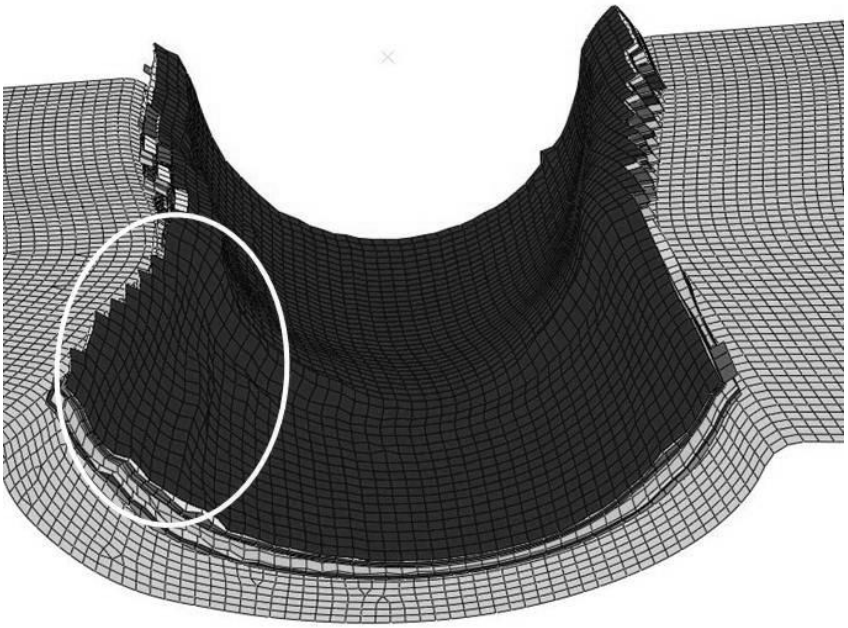

Figure B-21. Wave defect in root section after the application of vacuum pressure

Summary

A discrete mesoscopic approach using 1-D beam and 2-D shell elements was used in the commercially available finite element software, Abaqus, to model the mechanical behavior of six different non-crimp fabrics (NCFs) used in a 9-m long wind turbine blade (CX-100) manufactured by TPI Composites in Warren, RI. Simulations were performed to mimic the hand-layup of the several plies during the manufacturing process. Upon inspection of the deformed layers, none of the fabrics experienced excessive in-plane shearing to conform to the molds of the blade, but some small in-plane waviness was observed. Similarly, the yarns of the fabric layers were shown to be below the tensile load breaking threshold. After all of the layers were pressed into the low-pressure and high-pressure molds of the wind turbine blade, a pressure equivalent to atmospheric

pressure was applied onto the top-fabric surfaces to simulate the vacuum compaction stage of the manufacturing process. During this stage in the process, it was shown that the bending stiffness of the material as well as the friction between layers and the location of ply drops were parameters that could influence the formation of out-of-plane wave defects. However, when representing the actual CX-100 design, the simulation confirmed that the design was not vulnerable to manufacturing-induced wave defects. With or without defects, the modeling approach presented in this research allowed for the reorientation of the fabric yarns to be tracked during the manufacturing process.

LITERATURE CITED

[1] Nolet, S. 2010
TPI Composites, Inc.
Personal communication, February.

[2] LeBlanc, B.: "Non-destructive Inspection of Wind Turbine Blades with Three Dimensional Digital Image Correlation", Master's Thesis, Dept. of Mechanical Engineering, University of Massachusetts Lowell, 2011.

[3] Klute, S.M., Sang, A.K., Gifford, D.K., and Froggatt, M.E.: "Defect Detection During Manufacture of Composite Wind Turbine Blade with Embedded Fiber Optic Distributed Strain Sensor," SAMPE Tech Conference & Exhibition, Fort Worth, Texas (USA), 2011.